

# Soft Gluon Resummation Effects in Single Graviton Production at the CERN Large Hadron Collider in the Randall-Sundrum Model

Qiang Li\*, Chong Sheng Li†, and Li Lin Yang‡

*Department of Physics, Peking University, Beijing 100871, China*

## Abstract

We study QCD effects in single graviton production at the CERN Large Hadron Collider (LHC) in the Randall-Sundrum (RS) Model. We present in detail the complete next-to-leading order (NLO) QCD corrections to the inclusive total cross sections. The NLO QCD corrections enhance significantly the total cross sections and decrease efficiently the dependence of the total cross sections on the factorization and renormalization scales. We also examine the uncertainty of the total cross sections due to the parton distribution function (PDF) uncertainties. For the differential cross sections on the transverse momentum ( $q_T$ ) of the graviton, within the CSS resummation formalism, we resum the logarithmically-enhanced terms at small  $q_T$  to all orders up to NLO logarithmic accuracy. Combined with the fixed order calculations, we give consistent predictions for both small  $q_T$  and large  $q_T$ .

PACS numbers: 11.10.Kk, 12.38.-t, 12.38.Bx, 13.85.Qk

---

\* Electronics address: qliphy@pku.edu.cn

† Electronics address: csli@pku.edu.cn

‡ Electronics address: llyang@pku.edu.cn

## I. INTRODUCTION

Now search for extra dimensions has been one of the major objects at the LHC, since its physical effects can appear at the TeV energy scale. The idea of extra dimensions was revived in the 1990's[1, 2, 3, 4, 5, 6], which can bring new solutions to the gauge hierarchy problem and be used to resolve some problems of the SM such as the origin of the fermion masses and their hierarchy.

So far, there have been various extra dimension models, which can be divided into two major classes according to the geometry of the background space-time manifold. The first one includes the ADD model[1] and its variants, which extend the dimension of the total space-time to  $D = 4 + \delta$ , propose a factorizable metric, and get large size of the extra dimensions ( $\gg 1/M_p$ ). In the ADD model, the SM particles live in the usual 4-dimensional space-time, while gravity can propagate in the additional  $\delta$ -dimensional space, which is assumed for simplicity to be compactified on the  $\delta$ -dimensional torus  $T^\delta$  with a common radius  $R$ . Then the 4-dimensional Planck scale  $M_p$  is related to the fundamental scale  $M_s$  as follows[1, 7]:

$$M_p^2 = M_s^{\delta+2}(2\pi R)^\delta, \quad (1)$$

where  $M_s \sim \text{TeV}$ . According to Eq. (1), deviations from the usual Newtonian gravitational force law can be expected at distances smaller than  $R \sim 2 \times 10^{-17} \times 10^{\frac{32}{\delta}} \text{cm}$ [7]. For  $\delta \geq 2$ , ADD is consistent with the current experiments[8] since gravitational forces are not yet well probed at distances less than about a millimeter. However for  $\delta = 2$ , there are constraints arising from, e.g., supernova cooling, which require  $M_s \geq 10 - 100\text{TeV}$  if  $\delta = 2$  [7].

The second one includes the 5-dimensional RS model[2] and its variants, in which a warped metric is introduced and the size of the extra dimension needs not to be too large compared with the Planck length. In the RS model, the extra dimension is assumed to be an  $S_1/Z_2$  orbifold, which has two fixed points,  $\theta = 0$  and  $\theta = \pi$ . At each fixed point, there is a 3-brane, and the brane at  $\theta = \pi$  corresponds to the brane we live on, while the one at  $\theta = 0$  is the high energy brane. Between the two 3-branes is a slice of AdS space, where only the graviton can propagate into. Moreover, the 4-dimensional metric is the function of the coordinate of the 5th dimension, i.e.

$$ds^2 = e^{-2kr_c|\phi|}(\eta_{\mu\nu} + \frac{2}{M_*^{3/2}}h_{\mu\nu})dx^\mu dx^\nu - r_c^2 d\phi^2, \quad 0 \leq |\phi| \leq \pi, \quad (2)$$

where  $k$  is a scale of order of the Planck scale and relates the 5-dimensional Planck scale  $M_*$  to the cosmological constant,  $r_c$  is the compactification radius, and  $h_{\mu\nu}$  is the graviton.

After solving the 5-dimensional Einstein equation, we can get the tensions of the two branes[7]

$$V_0 = -V_\pi = 12kM_*^3, \quad (3)$$

and from Eq.(2), we can get the relation between  $M_*$  and 4-dimensional reduced Planck scale  $\overline{M}_P$ [2]

$$\overline{M}_P^2 = \frac{M_*^3}{k}(1 - e^{-2kr_c\pi}), \quad (4)$$

from which we can see that for moderately large values of the compactification scale  $r_c$ , the relation between  $M_*$  and  $\overline{M}_P$  almost does not depend on  $r_c$ , and it is completely different from the results in the ADD model. Compared with the ADD model, the RS model present a different solution to the gauge Hierarchy problem: the physical mass  $m$  of a field on the brane where our world live on, is related to the fundamental mass parameter  $m_0$  as following

$$m = e^{-kr_c\pi}m_0, \quad (5)$$

thus the hierarchy problem can be solved if  $kr_c \sim 12$ .

In the RS model, there also exist KK towers of massive spin-2 gravitons which can interact with the SM fields, and we have the following 4-dimensional effective Lagrangian[9, 10]:

$$\mathcal{L} = -\frac{1}{\overline{M}_P}T^{\alpha\beta}(x)h_{\alpha\beta}^{(0)}(x) - \frac{1}{\Lambda_\pi}T^{\alpha\beta}(x)\sum_{n=1}^{\infty}h_{\alpha\beta}^{(n)}(x) \quad (6)$$

where

$$\Lambda_\pi = e^{-kr_c\pi}\overline{M}_P = \frac{m_1\overline{M}_P}{x_1k}, \quad (7)$$

and is at the electroweak scale. Thus the coupling of the massless graviton  $h^{(0)}$  is suppressed by the Planck scale, and the ones of the massive graviton  $h^{(n)}$  by  $\Lambda_\pi$ , but which is only TeV. The masses of the  $n$ th graviton KK excitation modes are also at the electroweak scale, which are given by

$$m_n = kx_n e^{-kr_c\pi} = m_1 \frac{x_n}{x_1}, \quad (8)$$

where the  $x_n$ 's are the  $n$ th roots of the first order Bessel function.

From Eqs.(7) and (8), the graviton sector of the RS model is completely determined by the two parameters  $m_1$  and  $k/\overline{M}_P$ . Current constraints[10, 11, 12] for the parameters of the

RS model are from the theoretical requirement, the low energy precise measurement and also the data from Tevatron, from which we expect  $0.01 \leq k/\overline{M}_P < 0.1$  and  $\Lambda_\pi \leq 10$  TeV.

There are two classes of effects that can be used to probe extra dimension in the RS model at high energy colliders: real graviton emission and virtual KK tower exchange. In the RS model, the lightest massive graviton can have a mass of several hundred GeV, and may be produced copiously at the LHC. More importantly, it has much larger couplings to the SM particles than the ones in the ADD model, thus it may decay into observable particles and hence be detected. And there have been detailed analysis[13] which demonstrate that using channels  $pp \rightarrow h^{(n)} \rightarrow e^+e^-, \gamma\gamma, \dots$ , we can probe the massive graviton in the RS model with masses up to several TeV. However, those analysis[13] are based on the LO results, in order to improve the precision of the theoretical predictions, the higher order QCD effects are necessary. In the ADD model and the RS model, the NLO QCD corrections to the virtual graviton production at the LHC have been discussed in Ref.[12], however, the K factors contributed from different parts, the scale dependence and the PDF uncertainty for above processes needs further studies. Moreover, they also did not consider the kinematic distribution of the events, which is very important in designing the strategy of discovery. In this paper, we study the transverse momentum distribution of the massive graviton at NLO in QCD, and all order soft gluon resummation effects on the distribution to give reasonable predictions.

The arrangement of this paper is as follows. In Sect. II, we show the LO results and define the notations. In Sect. III, we present the details of the calculations of both the virtual and real parts of the NLO QCD corrections. In Sect. IV, we give the transverse momentum distribution. In Sect. V, we present the detailed numerical results for the total cross sections and also the transverse momentum distribution. Sec. VI contains a brief conclusion.

## II. LEADING ORDER CALCULATIONS

The related Feynman diagrams which contribute to the LO amplitude of the partonic process  $g_p^a(p_1)g_\sigma^b(p_2), q_r(p_1)\bar{q}_s(p_2) \rightarrow h_{\mu\nu}^{(n)}$  are shown in Fig. 1. The relevant Feynman rules can be read easily from the ones in the ADD model presented in Ref.[12, 14], from which

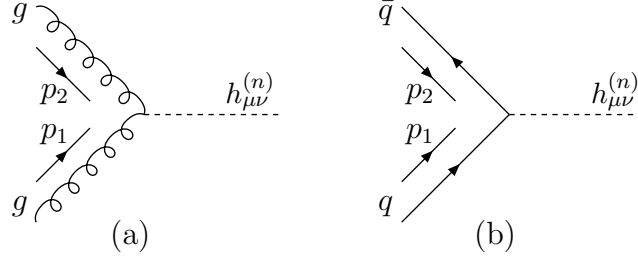


FIG. 1: Leading order Feynman diagrams for  $pp \rightarrow h_{\mu\nu}^{(n)}$ .

we can get the LO amplitude in  $n = 4 - 2\epsilon$  dimensions as following

$$M_{gg}^{(0)} = -\frac{i\delta_{ab}\mu_r^{4-n}}{\Lambda_\pi} \times \left[ p_1 \cdot p_2 C_{\mu\nu,\rho\sigma} + D_{\mu\nu,\rho\sigma} + E_{\mu\nu,\rho\sigma}(p_1, p_2) \right] \epsilon_\rho^a(p_1) \epsilon_\sigma^b(p_2) \epsilon_{\mu\nu}^{s*}(p_1 + p_2), \quad (9)$$

$$M_{q\bar{q}}^{(0)} = -\frac{i\delta_{rs}\mu_r^{4-n}}{4\Lambda_\pi} \times \bar{v}(p_2) \left[ \gamma_\mu(p_{1\nu} - p_{2\nu}) + \gamma_\nu(p_{1\mu} - p_{2\mu}) - 2\eta_{\mu\nu}(\not{p}_1 - \not{p}_2 - 2m_q) \right] u(p_1) \epsilon_{\mu\nu}^{s*}(p_1 + p_2), \quad (10)$$

where  $\delta_{ab}$  and  $\delta_{rs}$  are color tensors ( $a, b$  are the color indices of the initial state gluons, and  $r, s$  are the color indices of the initial state quarks),  $C_{\mu\nu,\rho\sigma}$ ,  $D_{\mu\nu,\rho\sigma}$  and  $E_{\mu\nu,\rho\sigma}(p_1, p_2)$  are the coefficients in the couplings between the graviton and gluons, which can be found in Ref.[14],  $\mu_r$  is a mass parameter introduced to keep the couplings dimensionless.

For the polarization sum of the massive graviton, we have[12, 14]

$$\sum_{s=1}^5 \epsilon_{\mu\nu}^s(k) \epsilon_{\alpha\beta}^{s*}(k) = P_{\mu\nu\alpha\beta}, \quad (11)$$

where

$$P_{\mu\nu\alpha\beta} = \frac{1}{2} \left( \eta_{\mu\alpha} \eta_{\nu\beta} + \eta_{\mu\beta} \eta_{\nu\alpha} - \frac{2}{n-1} \eta_{\mu\nu} \eta_{\alpha\beta} \right) + \dots, \quad (12)$$

the dots represent terms proportional to the graviton momentum  $k_\mu$ , and since  $k^\mu T_{\mu\nu} = 0$ , give a vanishing contribution to the amplitude. For convenience, below we define

$$\chi \equiv \frac{2}{n-1} = \frac{2}{3-2\epsilon}. \quad (13)$$

Moreover, in order to avoid introducing external ghost lines while summing over the gluon helicities, we limit ourselves to the sum over the physical polarizations of the gluons [15],

i.e.

$$P_i^{\mu\nu} = \sum_T \epsilon_T^\mu(k_i) \epsilon_T^\nu(k_i) = -g^{\mu\nu} + \frac{n_i^\mu k_i^\nu + k_i^\mu n_i^\nu}{n_i \cdot k_i} - \frac{n_i^\mu k_i^\mu k_i^\nu}{(n_i \cdot k_i)^2}, \quad (14)$$

where the index  $i$  ( $=1,2$ ) labels the two external gluons, and  $n_i \neq k_i$  is an arbitrary vector.

This polarization sum obeys the transversality relations

$$k_{i\mu} P^{\mu\nu} = P^{\mu\nu} k_{i\nu} = n_{i\mu} P^{\mu\nu} = P^{\mu\nu} n_{i\nu} = 0. \quad (15)$$

Thus we can get the LO squared matrix element as following, in which the colors and spins of the outgoing particles have been summed:

$$\overline{|M_{gg}^{(0)}|^2} = \frac{1}{2(1-\epsilon)} \times \frac{1}{2(1-\epsilon)} \times \frac{1}{8} |M_{gg}^{(0)}|^2 = \frac{(2-\epsilon)\pi}{32\Lambda_\pi^2} s^2, \quad (16)$$

$$\overline{|M_{q\bar{q}}^{(0)}|^2} = \frac{1}{2} \times \frac{1}{2} \times \frac{1}{3} \times |M_{q\bar{q}}^{(0)}|^2 = \frac{(1-\epsilon)\pi}{24\Lambda_\pi^2} s^2, \quad (17)$$

where  $s \equiv (p_1 + p_2)^2$ .

Then the relevant partonic cross sections are

$$\hat{\sigma}_{gg}^{(LO)} = \frac{1}{2s} 2\pi \delta(s - m_n^2) \overline{|M_{gg}^{(0)}|^2} = \frac{(2-\epsilon)\pi}{32\Lambda_\pi^2} \delta(1 - \hat{\tau}), \quad (18)$$

$$\hat{\sigma}_{q\bar{q}}^{(LO)} = \frac{1}{2s} 2\pi \delta(s - m_n^2) \overline{|M_{q\bar{q}}^{(0)}|^2} = \frac{(1-\epsilon)\pi}{24\Lambda_\pi^2} \delta(1 - \hat{\tau}), \quad (19)$$

where  $\hat{\tau} \equiv m_n^2/s$ .

The LO total cross sections at the LHC are obtained by convoluting the partonic cross sections with the parton distribution functions (PDFs)  $G_{q,\bar{q},g/p}$  in the proton:

$$\sigma^{(LO)} \equiv \sigma_{gg}^{(LO)} + \sigma_{q\bar{q}}^{(LO)},$$

$$\sigma_{gg}^{(LO)} = \int_{\tau_0}^1 dx_1 \int_{\tau_0/x_1}^1 dx_2 \frac{1}{2} \left[ G_{g/p}(x_1, \mu_f) G_{g/p}(x_2, \mu_f) + G_{g/p}(x_2, \mu_f) G_{g/p}(x_1, \mu_f) \right] \hat{\sigma}_{gg}^{(LO)}, \quad (20)$$

$$\sigma_{q\bar{q}}^{(LO)} = \int_{\tau_0}^1 dx_1 \int_{\tau_0/x_1}^1 dx_2 \left[ G_{q/p}(x_1, \mu_f) G_{\bar{q}/p}(x_2, \mu_f) + G_{q/p}(x_2, \mu_f) G_{\bar{q}/p}(x_1, \mu_f) \right] \hat{\sigma}_{q\bar{q}}^{(0)}, \quad (21)$$

where  $\tau_0 \equiv m_n^2/S_0$ ,  $S_0 = (14\text{TeV})^2$  and  $\mu_F$  is the factorization scale.

### III. NEXT-TO-LEADING ORDER CALCULATIONS

The NLO QCD corrections consist of the following contributions: the virtual corrections arising from loop diagrams of colored particles, the real contributions arising from the radiation of a real gluon or a massless (anti)quark, and the contributions of mass factorization.

In the following, we will calculate these contributions separately. We use dimensional regularization (DREG)[16] in  $d = 4 - 2\epsilon$  dimensions to regulate the ultraviolet (UV) and infrared (IR) divergences.

### A. Virtual corrections

The virtual corrections to  $gg \rightarrow h_{\mu\nu}^{(n)}$  and  $q\bar{q} \rightarrow h_{\mu\nu}^{(n)}$  arise from the Feynman diagrams shown in Fig. 2 and Fig. 3. They consist of vertex diagrams arising from quarks, gluons and ghosts.

For the partonic cross section, the total virtual corrections can be written as

$$\hat{\sigma}_{gg,q\bar{q}}^V = \hat{\sigma}_{gg,q\bar{q}}^{unren} + \hat{\sigma}_{gg,q\bar{q}}^{con}, \quad (22)$$

where the first part in the right hand contains the radiative corrections from the one-loop vertex box diagrams shown in Fig. 2 and Fig. 3 (we have omitted the terms in proportional to  $m_t^2/m_n^2$ ):

$$\begin{aligned} \hat{\sigma}_{gg}^{unren} = 2C_\epsilon \frac{g_s^2(2-\epsilon)}{32\pi\Lambda_\pi^2} \delta(1-\hat{\tau}) \times & \left( \frac{-3}{8} \frac{1}{\epsilon_{IR}^2} - \frac{33}{48} \frac{1}{\epsilon_{IR}} + \frac{n_f}{24} \frac{1}{\epsilon_{IR}} + \frac{n_f}{24} \frac{1}{\epsilon_{UV}} - \frac{13}{48} \frac{1}{\epsilon_{UV}} \right. \\ & \left. + \frac{1}{8}\pi^2 - \frac{203}{96} + \frac{35n_f}{288} \right), \end{aligned} \quad (23)$$

$$\hat{\sigma}_{q\bar{q}}^{unren} = 2C_\epsilon \frac{g_s^2(1-\epsilon)}{24\pi\Lambda_\pi^2} \delta(1-\hat{\tau}) \times \left( \frac{-1}{6} \frac{1}{\epsilon_{IR}^2} - \frac{1}{3} \frac{1}{\epsilon_{IR}} + \frac{1}{12} \frac{1}{\epsilon_{UV}} + \frac{1}{18}\pi^2 - \frac{5}{6} \right), \quad (24)$$

where  $n_f = 5$  and  $C_\epsilon \equiv \frac{\Gamma(1-\epsilon)}{\Gamma(1-2\epsilon)} \left( \frac{4\pi\mu_r^2}{m_n^2} \right)^\epsilon$ , while the second part in the right hand of Eq.(22) is the contributions from the counterterms,

$$\hat{\sigma}_{gg}^{con} = 2\delta Z_g \hat{\sigma}_{gg}^{(0)} = 2C_\epsilon \times \left[ \frac{\alpha_s}{2\pi} \left( \frac{n_f}{3} - \frac{5}{2} \right) \left( \frac{1}{\epsilon_{IR}} - \frac{1}{\epsilon_{UV}} \right) - \frac{\alpha_s}{6\pi} \frac{1}{\epsilon_{UV}} \right] \times \frac{(2-\epsilon)\pi}{32\Lambda_\pi^2} \delta(1-\hat{\tau}), \quad (25)$$

$$\hat{\sigma}_{q\bar{q}}^{con} = 2\delta Z_q \hat{\sigma}_{q\bar{q}}^{(0)} = 2C_\epsilon \times \frac{\alpha_s}{3\pi} \left( \frac{1}{\epsilon_{IR}} - \frac{1}{\epsilon_{UV}} \right) \times \frac{(1-\epsilon)\pi}{24\Lambda_\pi^2} \delta(1-\hat{\tau}), \quad (26)$$

where  $\delta Z_g$  and  $\delta Z_q$  are the wavefunction renormalization constant for the external fields, fixed by on-shell subtraction,

$$\begin{aligned} \delta Z_g &= -\frac{\alpha_s}{2\pi} C_\epsilon \left( \frac{n_f}{3} - \frac{5}{2} \right) \left( \frac{1}{\epsilon_{UV}} - \frac{1}{\epsilon_{IR}} \right) - \frac{\alpha_s}{6\pi} C_\epsilon \frac{1}{\epsilon_{UV}}, \\ \delta Z_q &= \frac{-\alpha_s}{3\pi} C_\epsilon \left( \frac{1}{\epsilon_{UV}} - \frac{1}{\epsilon_{IR}} \right), \end{aligned}$$

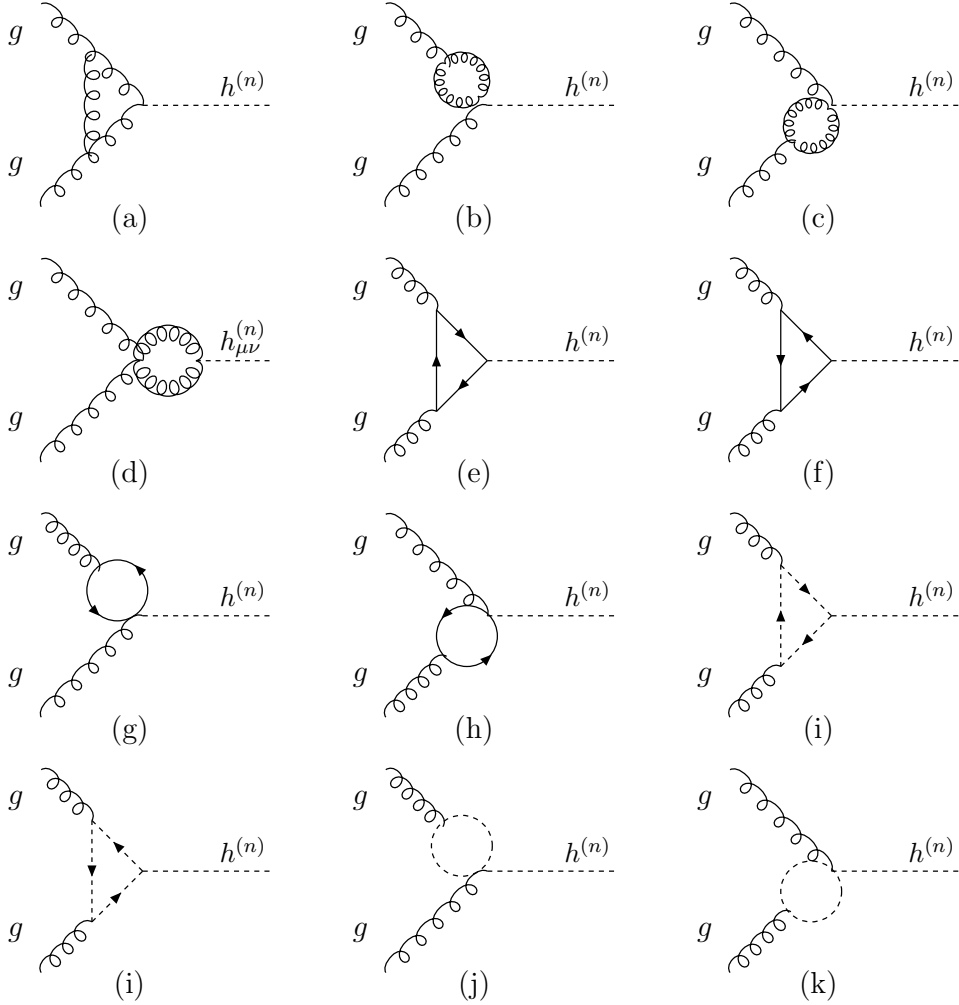


FIG. 2: One-loop virtual diagrams for  $gg \rightarrow h_{\mu\nu}^{(n)}$ .

The  $\mathcal{O}(\alpha_s)$  virtual corrections to the partonic cross section can be expressed as

$$\hat{\sigma}_{gg}^V = 2C_\epsilon \frac{g_s^2(2-\epsilon)}{32\pi\Lambda_\pi^2} \delta(1-\hat{\tau}) \times \left( \frac{-3}{8} \frac{1}{\epsilon_{IR}^2} - \frac{33}{48} \frac{1}{\epsilon_{IR}} + \frac{n_f}{24} \frac{1}{\epsilon_{IR}} + \frac{1}{8}\pi^2 - \frac{203}{96} + \frac{35n_f}{288} \right), \quad (27)$$

$$\hat{\sigma}_{q\bar{q}}^V = 2C_\epsilon \frac{g_s^2(1-\epsilon)}{24\pi\Lambda_\pi^2} \delta(1-\hat{\tau}) \times \left( \frac{-1}{6} \frac{1}{\epsilon_{IR}^2} - \frac{1}{3} \frac{1}{\epsilon_{IR}} + \frac{1}{18}\pi^2 - \frac{5}{6} \right), \quad (28)$$

which is UV finite, but still contains the IR divergences. Here, the IR divergences include the soft divergences and the collinear divergences. The soft divergences are canceled after adding the real emission corrections, and the remaining collinear divergences can be absorbed into the redefinition of PDF [17], which will be discussed in the following subsections.

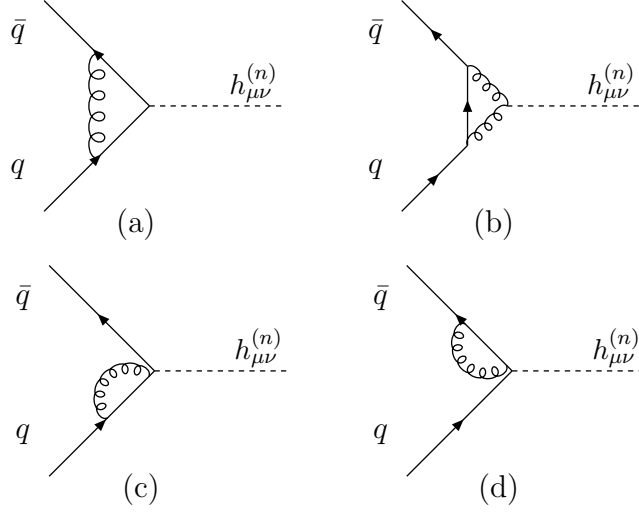


FIG. 3: One-loop virtual diagrams for  $q\bar{q} \rightarrow h_{\mu\nu}^{(n)}$ .

## B. Real corrections

The real corrections consist of the contributions from the radiation of a real gluon or a massless (anti)quark. The Feynman diagrams for the real gluon emission sub-process  $gg, q\bar{q} \rightarrow h_{\mu\nu}^{(n)}$  are shown in Fig. 4 and Fig. 5, respectively. The Feynman diagrams for massless (anti)quark emission (the diagrams for the antiquark emission sub-processes are similar and omitted here) are shown in Fig. 6

For the real gluon emission sub-processes  $g(p_1)g(p_2), q(p_1)\bar{q}(p_2) \rightarrow g(p_3)h_{\mu\nu}^{(n)}$ , the partonic cross sections is

$$\hat{\sigma}_{gg,q\bar{q}}^{real} = \frac{1}{2s} \int \overline{|M_{gg,q\bar{q}}^{real}|^2} d\Gamma_2, \quad (29)$$

with

$$\begin{aligned} \overline{|M_{gg}^{real}|^2} &= \frac{3 \times 8}{8 \times 8} \frac{1}{4(1-\epsilon)^2} \frac{4g_s^2}{\Lambda_\pi^2} \frac{1}{tu} \times \left\{ \epsilon t^2 u [26 - 9(4-2\epsilon) - 2(-5 + 2(4-2\epsilon))\epsilon\chi] \right. \\ &\quad + \epsilon^2 \chi t u^2 [26 - 9(4-2\epsilon) - 2(-5 + 2(4-2\epsilon))] - \frac{(1-\epsilon)}{4} s^3 [16 - 6(4-2\epsilon) + 4\epsilon^2 \chi] \\ &\quad - \frac{(1-\epsilon)}{2} t^3 [16 - 6(4-2\epsilon) + 4\epsilon^2 \chi] - \frac{(1-\epsilon)}{2} s^2 (t+u) [16 - 6(4-2\epsilon) + 4\epsilon^2 \chi] \\ &\quad - \frac{(1-\epsilon)}{2} u^3 [16 - 6(4-2\epsilon) + 4\epsilon^2 \chi] - \frac{(1-\epsilon)}{4s} (t^2 + tu + u^2)^2 [16 - 6(4-2\epsilon) + 4\epsilon^2 \chi] \\ &\quad \left. + \frac{s}{2} [2\epsilon t u (26 - 9(4-2\epsilon) - 6\epsilon\chi) - \frac{3}{2} (1-\epsilon) (t^2 + u^2) [16 - 6(4-2\epsilon) + 4\epsilon^2 \chi]] \right\}, \quad (30) \end{aligned}$$

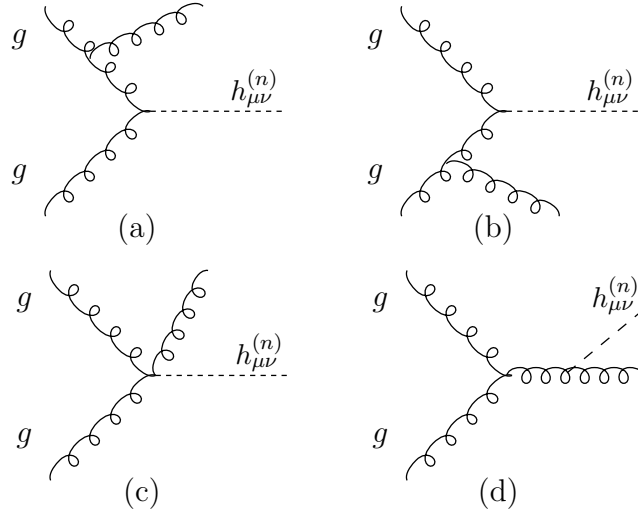


FIG. 4: Feynman diagrams of real gluon emission sub-processes  $gg \rightarrow h_{\mu\nu}^{(n)} + g$ .

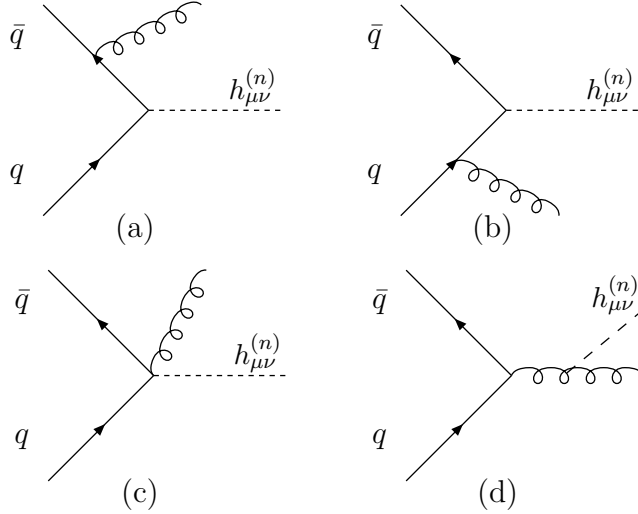


FIG. 5: Feynman diagrams of real gluon emission sub-processes  $q\bar{q} \rightarrow h_{\mu\nu}^{(n)} + g$ .

$$\begin{aligned}
\overline{|M_{q\bar{q}}^{real}|^2} &= \frac{4}{3} \frac{1}{3} \frac{1}{2} \frac{-g_s^2}{\Lambda_\pi^2} \frac{1}{stu} \times \left\{ 2(\epsilon - 1)s^4 + 4(\epsilon - 1)(t + u)s^3 \right. \\
&\quad - (\epsilon - 3)[(\epsilon - 1)t^2 + 2(3\epsilon - 2)ut + (\epsilon - 1)u^2]s^2 \\
&\quad - (t + u)[(\epsilon - 1)^2t^2 + (6\epsilon(\epsilon - 3) + 8)ut + (\epsilon - 1)^2u^2]s \\
&\quad \left. - 2tu[(\epsilon - 1)t^2 + 2\epsilon ut + (\epsilon - 1)u^2][\epsilon(\epsilon\chi + 3) - 2] \right\}, \tag{31}
\end{aligned}$$

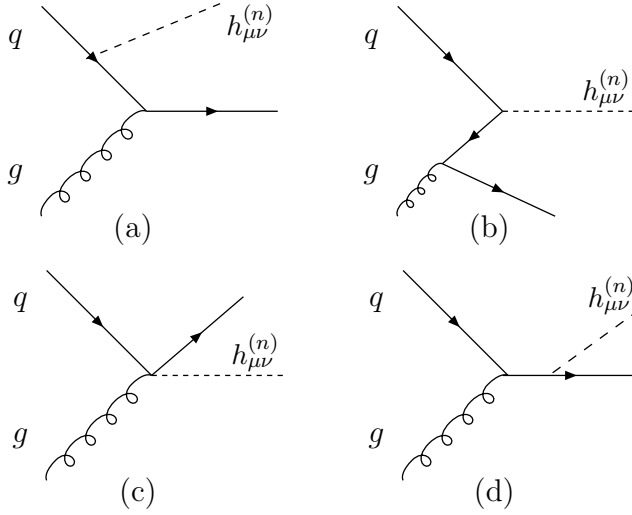


FIG. 6: Feynman diagrams of real quark emission sub-processes  $gq \rightarrow h_{\mu\nu}^{(n)} + q$ .

where  $\overline{|M_{gg,q\bar{q}}^{real}|^2}$  is the squared matrix of the real gluon emission sub-processes, in which the colors and spins of the outgoing particles have been summed, and the colors and spins of the incoming ones have been averaged over, and the final state 2-body phase space is

$$d\Gamma_2 = \frac{1}{8\pi\Gamma(1-\epsilon)} \left( \frac{4\pi\mu_r^2}{m_n^2} \right)^\epsilon (\hat{\tau})^\epsilon (1-\hat{\tau})^\epsilon \times v^{-\epsilon} (1-v)^{-\epsilon} dv, \quad (32)$$

where

$$v \equiv \frac{1}{2}(1 + \cos\theta), \quad (33)$$

$$t \equiv (p_1 - p_3)^2 = -s(1 - \hat{\tau})(1 - v), \quad (34)$$

$$u \equiv (p_2 - p_3)^2 = -s(1 - \hat{\tau})v, \quad (35)$$

and  $\theta$  is the the angle between the incoming gluon and the outgoing gluon.

After the phase space integration, we can get the partonic cross sections for the real gluon emission sub-processes,

$$\begin{aligned} \hat{\sigma}_{gg}^{real} = & \frac{(2-\epsilon)\alpha_s}{32\Lambda_\pi^2} C_\epsilon \frac{m_n^2}{s} \times \left\{ \frac{3}{\epsilon_{IR}^2} - \frac{6}{\epsilon_{IR}} \left[ \frac{\hat{\tau}}{(1-\hat{\tau})_+} + \frac{1-\hat{\tau}}{\hat{\tau}} + \hat{\tau}(1-\hat{\tau}) \right] \right. \\ & + 12 \left( \frac{\ln(1-\hat{\tau})}{1-\hat{\tau}} \right)_+ + 6 \left[ \frac{1-\hat{\tau}}{\hat{\tau}} + \hat{\tau}(1-\hat{\tau}) \right] \ln \left( \frac{(1-\hat{\tau})^2}{\hat{\tau}} \right) \\ & \left. - 6 \frac{\ln \hat{\tau}}{1-\hat{\tau}} - \frac{3}{2} - \frac{11}{2\hat{\tau}} + \frac{3}{2}\hat{\tau} + \frac{11\hat{\tau}^2}{2} \right\}, \end{aligned}$$

and

$$\hat{\sigma}_{q\bar{q}}^{real} = \frac{(1-\epsilon)\alpha_s}{24\Lambda_\pi^2} C_\epsilon \frac{m_n^2}{s} \times \left\{ \frac{4}{3\epsilon_{IR}^2} - \frac{1}{6\epsilon_{IR}} - \frac{4}{3\epsilon_{IR}} \frac{1+\hat{\tau}^2}{(1-\hat{\tau})_+} + \frac{16}{3} \left( \frac{\ln(1-\hat{\tau})}{1-\hat{\tau}} \right)_+ - \frac{4}{3} \ln \frac{(1-\hat{\tau})^2}{\hat{\tau}} - 2 \frac{\ln \hat{\tau}}{1-\hat{\tau}} + \frac{4}{3\hat{\tau}} - \frac{4\hat{\tau}^2}{3} \right\}. \quad (36)$$

The ‘‘plus’’ functions appearing in the above results are the distributions which satisfy the following equation:

$$\int_0^1 dz f_+(z) g(z) = \int_0^1 dz f(z) (g(z) - g(1)), \quad (37)$$

where  $g(z)$  is any well-behaved function in the region  $0 \leq z \leq 1$ .

Combining the contributions of the virtual corrections and the real gluon emission, we have

$$\begin{aligned} \hat{\sigma}_{gg}^{real} + \hat{\sigma}_{gg}^V &= \frac{(2-\epsilon)\alpha_s}{32\Lambda_\pi^2} C_\epsilon \frac{m_n^2}{s} \times \\ &\left\{ -\frac{6}{\epsilon_{IR}} \left[ \frac{\hat{\tau}}{(1-\hat{\tau})_+} + \frac{1-\hat{\tau}}{\hat{\tau}} + \hat{\tau}(1-\hat{\tau}) \right] - \frac{1}{\epsilon_{IR}} \left( \frac{11}{2} - \frac{n_f}{3} \right) \delta(1-\hat{\tau}) \right. \\ &+ \left( \pi^2 - \frac{203}{12} + \frac{35n_f}{36} \right) \delta(1-\hat{\tau}) + 12 \left( \frac{\ln(1-\hat{\tau})}{1-\hat{\tau}} \right)_+ \\ &+ 6 \left[ \frac{1-\hat{\tau}}{\hat{\tau}} + \hat{\tau}(1-\hat{\tau}) \right] \ln \left( \frac{(1-\hat{\tau})^2}{\hat{\tau}} \right) - 6 \frac{\ln \hat{\tau}}{1-\hat{\tau}} - \frac{3}{2} - \frac{11}{2\hat{\tau}} + \frac{3}{2} \hat{\tau} + \frac{11\hat{\tau}^2}{2} \left. \right\}, \quad (38) \end{aligned}$$

$$\begin{aligned} \hat{\sigma}_{q\bar{q}}^{real} + \hat{\sigma}_{q\bar{q}}^V &= \frac{(1-\epsilon)\alpha_s}{24\Lambda_\pi^2} C_\epsilon \frac{m_n^2}{s} \times \left\{ -\frac{4}{3} \frac{1}{\epsilon_{IR}} \left[ \frac{1+\hat{\tau}^2}{(1-\hat{\tau})_+} + \frac{3}{2} \delta(1-\hat{\tau}) \right] \right. \\ &+ \frac{4}{3} \left( -5 + \frac{\pi^2}{3} \right) \delta(1-\hat{\tau}) - \frac{4}{3\epsilon_{IR}} \frac{1+\hat{\tau}^2}{(1-\hat{\tau})_+} + \frac{16}{3} \left( \frac{\ln(1-\hat{\tau})}{1-\hat{\tau}} \right)_+ \\ &\left. - \frac{4}{3} \ln \frac{(1-\hat{\tau})^2}{\hat{\tau}} - 2 \frac{\ln \hat{\tau}}{1-\hat{\tau}} + \frac{4}{3\hat{\tau}} - \frac{4\hat{\tau}^2}{3} \right\}, \quad (39) \end{aligned}$$

note that the divergences appearing in above expressions are collinear, which can be absorbed into the redefinition of the PDF at NLO, in general called mass factorization [17]. This procedure in practice means that first we convolute the partonic cross section with the bare PDF  $G_{\alpha/p}(x)$ , and then rewrite  $G_{\alpha/p}(x)$  in terms of the renormalized PDF  $G_{\alpha/p}(x, \mu_f)$  in the numerical calculations. In the  $\overline{\text{MS}}$  scheme, the scale dependent PDF  $G_{\alpha/p}(x, \mu_f)$  is given by[18]

$$G_{\alpha/p}(x, \mu_f) = G_{\alpha/p}(x) + \sum_\beta \left( -\frac{1}{\epsilon} \right) \left[ \frac{\alpha_s}{2\pi} \frac{\Gamma(1-\epsilon)}{\Gamma(1-2\epsilon)} \left( \frac{4\pi\mu_r^2}{\mu_f^2} \right)^\epsilon \right] \int_x^1 \frac{dz}{z} P_{\alpha\beta}(z) G_{\beta/p}(x/z), \quad (40)$$

where  $P_{\alpha\beta}(z)$  are the leading order Altarelli-Parisi splitting functions [19]:

$$\begin{aligned}
P_{qq}^{(0)}(z) &= \frac{4}{3} \left[ \frac{1+z^2}{(1-z)_+} + \frac{3}{2} \delta(1-z) \right], \\
P_{qg}^{(0)}(z) &= \frac{1}{2} [(1-z)^2 + z^2], \\
P_{gq}^{(0)}(z) &= \frac{4}{3} \frac{(1-z)^2 + 1}{z}, \\
P_{gg}^{(0)}(z) &= 2N_c \left[ \frac{z}{(1-z)_+} + \frac{1-z}{z} + z(1-z) \right] + \left( \frac{11}{2} - \frac{n_f}{3} \right) \delta(1-z). \tag{41}
\end{aligned}$$

Here, for the real gluon emission sub-processes  $gg \rightarrow h_{\mu\nu}^{(n)}$  and  $q\bar{q} \rightarrow h_{\mu\nu}^{(n)}$ , we first consider only the contributions from  $p_{gg}$  and  $p_{qq}$ , and we can get the relevant counterterm arising from the PDF redefinition as following:

$$\delta\hat{\sigma}_{gg} = 2 \times \frac{\alpha_s}{2\pi} C'_\epsilon \frac{(2-\epsilon)}{32\Lambda_\pi^2} z P_{gg}^{(0)}(z), \tag{42}$$

$$\delta\hat{\sigma}_{q\bar{q}} = 2 \times \frac{\alpha_s}{2\pi} C'_\epsilon \frac{(1-\epsilon)}{24\Lambda_\pi^2} z P_{qq}^{(0)}(z), \tag{43}$$

where  $C'_\epsilon \equiv \frac{\Gamma(1-\epsilon)}{\Gamma(1-2\epsilon)} \left( \frac{4\pi\mu_f^2}{\mu_f^2} \right)^\epsilon$  and  $z \equiv m_n^2/(x_1 x_2 S) = \hat{\tau}$ .

Summing up the virtual, real emission and PDF redefinition contributions, we have the IR finite results

$$\begin{aligned}
\hat{\sigma}_{gg}^{NLO} &= \hat{\sigma}_{gg}^{real} + \hat{\sigma}_{gg}^V + \delta\hat{\sigma}_{gg} = \frac{(2-\epsilon)\alpha_s}{32\Lambda_\pi^2} C_\epsilon \frac{m_n^2}{s} \times \\
&\left\{ 6 \ln \left( \frac{m_n^2}{\mu_f^2} \right) \left[ \frac{\hat{\tau}}{(1-\hat{\tau})_+} + \frac{1-\hat{\tau}}{\hat{\tau}} + \hat{\tau}(1-\hat{\tau}) \right] + \ln \left( \frac{m_n^2}{\mu_f^2} \right) \left( \frac{11}{2} - \frac{n_f}{3} \right) \delta(1-\hat{\tau}) \right. \\
&+ \left( \pi^2 - \frac{203}{12} + \frac{35n_f}{36} \right) \delta(1-\hat{\tau}) + 12 \left( \frac{\ln(1-\hat{\tau})}{1-\hat{\tau}} \right)_+ \\
&\left. + 6 \left[ \frac{1-\hat{\tau}}{\hat{\tau}} + \hat{\tau}(1-\hat{\tau}) \right] \ln \left( \frac{(1-\hat{\tau})^2}{\hat{\tau}} \right) - 6 \frac{\ln \hat{\tau}}{1-\hat{\tau}} - \frac{3}{2} - \frac{11}{2\hat{\tau}} + \frac{3}{2} \hat{\tau} + \frac{11\hat{\tau}^2}{2} \right\}, \tag{44}
\end{aligned}$$

$$\begin{aligned}
\hat{\sigma}_{q\bar{q}}^{NLO} &= \hat{\sigma}_{q\bar{q}}^{real} + \hat{\sigma}_{q\bar{q}}^V + \delta\hat{\sigma}_{q\bar{q}} = \frac{(1-\epsilon)\alpha_s}{24\Lambda_\pi^2} C_\epsilon \frac{m_n^2}{s} \\
&\times \left\{ -\frac{4}{3} \ln \left( \frac{m_n^2}{\mu_f^2} \right) \left[ \frac{1+\hat{\tau}^2}{(1-\hat{\tau})_+} + \frac{3}{2} \delta(1-\hat{\tau}) \right] \right. \\
&+ \frac{4}{3} \left( -5 + \frac{\pi^2}{3} \right) \delta(1-\hat{\tau}) - \frac{4}{3\epsilon_{IR}} \frac{1+\hat{\tau}^2}{(1-\hat{\tau})_+} + \frac{16}{3} \left( \frac{\ln(1-\hat{\tau})}{1-\hat{\tau}} \right)_+ \\
&\left. - \frac{4}{3} \ln \frac{(1-\hat{\tau})^2}{\hat{\tau}} - 2 \frac{\ln \hat{\tau}}{1-\hat{\tau}} + \frac{4}{3\hat{\tau}} - \frac{4\hat{\tau}^2}{3} \right\}. \tag{45}
\end{aligned}$$

For the real (anti-)quark emission sub-processes  $gq(\bar{q}) \rightarrow q(\bar{q})h_{\mu\nu}^{(n)}$ , the relevant results can be got in the similar way as above. First, the partonic cross sections is

$$\hat{\sigma}_{gq,g\bar{q}}^{real} = \frac{1}{2s} \int \overline{|M_{gq,g\bar{q}}^{real}|^2} d\Gamma_2, \quad (46)$$

with

$$\overline{|M_{gq}^{real}|^2} = -\frac{1}{1-\epsilon} \overline{|M_{q\bar{q}}^{real}|^2} (s \leftrightarrow t), \quad (47)$$

$$\overline{|M_{g\bar{q}}^{real}|^2} = -\frac{1}{1-\epsilon} \overline{|M_{q\bar{q}}^{real}|^2} (s \leftrightarrow u), \quad (48)$$

where  $\overline{|M_{gq,g\bar{q}}^{real}|^2}$  is the squared matrix of the real (anti-)quark emission sub-processes, in which the colors and spins of the outgoing particles have been summed, and the colors and spins of the incoming ones have been averaged over.

Secondly, the relevant counterterm arising from the PDF redefinition for real (anti-)quark emission sub-processes are shown as following, where we consider only the contributions from  $p_{gq}$  and  $p_{qg}$ :

$$\delta\hat{\sigma}_{gq} = \frac{\alpha_s}{2\pi} C'_\epsilon \frac{(1-\epsilon)}{24\Lambda_\pi^2} z P_{qg}^{(0)}(z) + 2 \times \frac{1}{2} \frac{\alpha_s}{2\pi} C'_\epsilon \frac{(2-\epsilon)}{32\Lambda_\pi^2} z P_{gq}^{(0)}(z). \quad (49)$$

Summing up the virtual, real emission and PDF redefinition contributions, again we get the IR finite results for real (anti-)quark emission sub-processes,

$$\begin{aligned} \hat{\sigma}_{gq}^{NLO} (= \hat{\sigma}_{g\bar{q}}^{NLO}) &= \hat{\sigma}_{gq}^{real} + \delta\hat{\sigma}_{gq} = \frac{\alpha_s}{96\Lambda_\pi^2} C'_\epsilon \frac{m_n^2}{s} \\ &\times \left\{ \left[ 4 \frac{1 + (1 - \hat{\tau})^2}{\hat{\tau}} + ((1 - \hat{\tau})^2 + \hat{\tau}^2) \right] \ln \left( \frac{m_n^2}{\mu_f^2} \right) \right. \\ &\left. + \left[ 4 \frac{1 + (1 - \hat{\tau}^2)}{\hat{\tau}} + ((1 - \hat{\tau})^2 + \hat{\tau}^2) \right] \ln \left( \frac{(1 - \hat{\tau})^2}{\hat{\tau}} \right) + \frac{9}{2} - \frac{6}{\hat{\tau}} + 9\hat{\tau} - \frac{7\hat{\tau}^2}{2} \right\}. \quad (50) \end{aligned}$$

Finally, the NLO total cross section for  $pp \rightarrow h^{(n)}$  in the  $\overline{MS}$  factorization scheme is obtained by summing up the Born, virtual, real emission and PDF redefinition contributions. In terms of the above notations, we have

$$\begin{aligned} \sigma^{(NLO)} &= \sigma_{gg}^{(LO)} + \sigma_{q\bar{q}}^{(LO)} + \sigma_{gg}^{(NLO)} + \sigma_{q\bar{q}}^{(NLO)} + \sigma_{gq}^{(NLO)} + \sigma_{g\bar{q}}^{(NLO)} \\ &= \sigma_{gg}^{(LO)} + \sigma_{q\bar{q}}^{(LO)} \\ &+ \int_{\tau_0}^1 dx_1 \int_{\tau_0/x_1}^1 dx_2 \frac{1}{2} \left[ G_{g/p}(x_1, \mu_f) G_{g/p}(x_2, \mu_f) + G_{g/p}(x_2, \mu_f) G_{g/p}(x_1, \mu_f) \right] \hat{\sigma}_{gg}^{(NLO)} \end{aligned}$$

$$\begin{aligned}
& + \int_{\tau_0}^1 dx_1 \int_{\tau_0/x_1}^1 dx_2 \left[ G_{q/p}(x_1, \mu_f) G_{\bar{q}/p}(x_2, \mu_f) + G_{q/p}(x_2, \mu_f) G_{\bar{q}/p}(x_1, \mu_f) \right] \hat{\sigma}_{q\bar{q}}^{(NLO)} \\
& + \int_{\tau_0}^1 dx_1 \int_{\tau_0/x_1}^1 dx_2 \left[ G_{q/p}(x_1, \mu_f) G_{g/p}(x_2, \mu_f) + G_{q/p}(x_2, \mu_f) G_{g/p}(x_1, \mu_f) \right] \hat{\sigma}_{gq}^{(NLO)} \\
& + \int_{\tau_0}^1 dx_1 \int_{\tau_0/x_1}^1 dx_2 \left[ G_{g/p}(x_1, \mu_f) G_{\bar{q}/p}(x_2, \mu_f) + G_{g/p}(x_2, \mu_f) G_{\bar{q}/p}(x_1, \mu_f) \right] \hat{\sigma}_{g\bar{q}}^{(NLO)}. \quad (51)
\end{aligned}$$

### C. Transverse momentum distribution

In this section we investigate the transverse momentum distribution of the massive graviton. At LO the graviton is kept at zero  $q_T$  due to momentum conservation and the distribution is proportional to  $\delta^2(\vec{q}_T)$ . Thus the LO distribution at non-zero  $q_T$  belongs to  $\mathcal{O}(\alpha_s)$ , where momentum conservation is retained by the additional parton emitted. The distribution can be obtained from the squared amplitudes of the real emission processes, i.e. Eqs. (30), (31) and (47). However, the corresponding fixed order result of the transverse momentum distribution is only valid when  $q_T$  is not too small compared with the mass of the massive graviton  $m_n$ . If  $q_T \ll m_n$ , the corresponding parton emitted would be either soft or collinear to one of the initial partons. Thus, large logarithms like  $\ln(m_n^2/q_T^2)$  will appear and will dominate over the cross section for sufficiently small  $q_T$ . In general, there should be double logarithms for each gluon attached to the initial quarks due to the overlap of soft region and collinear region. As a result, the perturbative expansion would be controlled by  $\alpha_s \ln^2(m_n^2/q_T^2)$  rather than  $\alpha_s$ . The convergence of the perturbation series will be spoiled if  $\alpha_s \ln^2(m_n^2/q_T^2)$  approaches unity. In order to make use of the perturbation theory with the existence of large logarithms at each order, one must reorganize the perturbative expansion to resum the large terms. In this paper, we use the Collins-Soper-Sterman (CSS) resummation formalism[20] to calculate all order soft gluon effects on the transverse momentum distribution.

In the CSS formalism, the differential cross section we are considering can be written as

$$\frac{d\sigma}{dq_T^2 dy}(\text{total}) = \frac{d\sigma}{dq_T^2 dy}(\text{resum}) + Y(q_T, m, x_1^0, x_2^0), \quad (52)$$

where

$$\frac{d\sigma}{dq_T^2 dy}(\text{resum}) = \sum_{\alpha, \beta} \frac{d\sigma_{\alpha\beta}}{dq_T^2 dy}(\text{resum}) \quad (53)$$

$$Y(q_T, m, x_1^0, x_2^0) = \sum_{ab} Y_{ab}(q_T, m, x_1^0, x_2^0), \quad (54)$$

and the resummed part can be expressed as an inverse Fourier transformation

$$\begin{aligned}\frac{d\sigma_{\alpha\beta}}{dq_T^2 dy}(\text{resum}) &= \frac{1}{2}\sigma_{\alpha\beta}^0 \frac{1}{2\pi} \int d^2\vec{b} \exp(i\vec{b} \cdot \vec{q}_T) W_{\alpha\beta}(b, m, x_1^0, x_2^0) \\ &= \sum_{\alpha,\beta} \frac{1}{2}\sigma_{\alpha\beta}^0 \int_0^\infty b db J_0(bq_T) W_{\alpha\beta}(b, m, x_1^0, x_2^0),\end{aligned}\quad (55)$$

with

$$\begin{aligned}W_{\alpha\beta}(b, m, x_1^0, x_2^0) &= \tilde{f}_{\alpha/A}(x_1^0, C_3/b) \tilde{f}_{\beta/B}(x_2^0, C_3/b) \\ &\times \exp \left\{ - \int_{C_1^2/b^2}^{C_2^2 m^2} \frac{d\bar{\mu}^2}{\bar{\mu}^2} \left[ \ln \frac{C_2^2 m^2}{\bar{\mu}^2} A(\alpha_s(\bar{\mu})) + B(\alpha_s(\bar{\mu})) \right] \right\},\end{aligned}\quad (56)$$

where  $\alpha\beta = gg, q\bar{q}$ ,  $ab = gg, q\bar{q}, q(\bar{q})g$ ,  $\vec{b}$  is the impact parameter conjugating to  $\vec{q}_T$ ,  $J_0$  is zero order Bessel function of the first kind, and  $x_1^0 = e^y m_n / \sqrt{s}$ ,  $x_2^0 = e^{-y} m_n / \sqrt{s}$ . Here  $C_i (i = 1, 2, 3)$  are constants of order 1 which are by convention [20] chosen to be

$$C_1 = C_3 = 2e^{-\gamma_E} \equiv b_0, \quad C_2 = 1, \quad (57)$$

and  $\tilde{f}$  is the convolution of the PDFs and the coefficient functions  $C$

$$\tilde{f}_{\alpha/h}(x, \mu) = \sum_\gamma \int_x^1 \frac{dz}{z} C_{\alpha\gamma}(z, \alpha_s(\mu)) f_{\gamma/h}(x, \mu), \quad (58)$$

and the coefficients  $A$ ,  $B$  and  $C$  can be expanded to series in  $\alpha_s$

$$A(\alpha_s) = \sum_{n=1}^{\infty} A^{(n)} \left( \frac{\alpha_s}{\pi} \right)^n, \quad (59)$$

$$B(\alpha_s) = \sum_{n=1}^{\infty} B^{(n)} \left( \frac{\alpha_s}{\pi} \right)^n, \quad (60)$$

$$C_{\alpha\beta}(z, \alpha_s) = \sum_{n=0}^{\infty} C_{\alpha\beta}^{(n)}(z) \left( \frac{\alpha_s}{\pi} \right)^n, \quad (61)$$

and they can be calculated order by order in perturbative theory. In our case, since the massive graviton is colorless, thus the lowest order coefficients is the same as the ones in the case of  $gg \rightarrow H^0$ [21] and Drell-Yan[22]. For the  $gg$  channel, we have

$$\begin{aligned}A^{(1)} &= 2N_c = 6, & B^{(1)} &= -2\beta_0 = (33 - 2n_f)/6, \\ C_{\alpha\beta}^{(0)}(z) &= \delta_{\alpha\beta} \delta(1-z),\end{aligned}\quad (62)$$

and for the  $q\bar{q}$  channel, we have

$$A^{(1)} = C_F = \frac{4}{3}, \quad B^{(1)} = -\frac{3}{2}C_F = -2, \quad (63)$$

$$C_{\alpha\beta}^{(0)}(z) = \delta_{\alpha\beta} \delta(1-z). \quad (64)$$

With these coefficients, we can actually sum up all terms like  $\alpha_s^n L^{2n-1}$  and  $\alpha_s^n L^{2n-2}$ .

However, the resummed part is still not able to be calculated perturbatively. The reason is that in Eq. (55), the integral over the impact parameter  $b$  extends to infinity, while the integrand involves the strong coupling constant  $\alpha_s$  and the PDFs at scale  $b_0/b$ , where they are not well defined if  $b$  is large enough so that  $b_0/b$  enters non-perturbative region. Collins, Soper and Sterman, in their original paper [20], suggested that one can use a cut-off  $b_{\max}$  and regard the effects from  $b > b_{\max}$  as non-perturbative input. Practically, they replacing  $W(b)$  in Eq. (55) by

$$\widetilde{W}(b) = W(b_*)F_{\text{NP}}(b), \quad (65)$$

where

$$b_* = \frac{b}{\sqrt{1 + (b/b_{\max})^2}}, \quad (66)$$

and  $F_{\text{NP}}(b)$  parameterizes the non-perturbative effects. Since  $b_*$  never exceeds  $b_{\max}$ ,  $W(b_*)$  can be calculated perturbatively, and the theoretical uncertainty mainly relies on the function  $F_{\text{NP}}$ . Recently, Landry, Brock, Nadolsky and Yuan (BLNY) [23] proposed the form

$$F_{\text{NP}} = \exp \left\{ -b^2 \left[ g_1 + g_2 \ln \frac{m}{2Q_0} + g_1 g_3 \ln(100x_1^0 x_2^0) \right] \right\}, \quad (67)$$

They take  $b_{\max} = 0.5\text{GeV}^{-1}$ ,  $Q_0 = 1.6\text{GeV}$  and the parameters  $g_i (i = 1, 2, 3)$  are fitted to the available Drell-Yan data, which are given by

$$g_1 = 0.21, \quad g_2 = 0.68, \quad g_3 = -0.60. \quad (68)$$

The another term in Eq. (53), the  $Y$  term, is the remaining contributions which are not resummed. Since it contains no large logarithms, it can be reliably computed by fixed order truncation of the perturbative series

$$Y_{ab} = \frac{d\sigma_{ab}}{dq_T^2 dy}(\text{pert}) - \frac{d\sigma_{ab}}{dq_T^2 dy}(\text{asym}), \quad (69)$$

where the first term in the right hand is the fixed-order perturbative results, and the second term is the asymptotic part of the differential cross section, defined as the terms which are at least as singular as  $1/q_T^2$  when  $q_T \rightarrow 0$ , which can be got by expanding the resummed part, i.e. Eq.(55). In our case, we have

$$\frac{d\sigma_{gg}}{dq_T^2 dy}(\text{asym}) = \frac{1}{2}\sigma_{gg}^0 \frac{\alpha_s}{2\pi} \frac{\tau_0}{q_T^2} \left\{ f_{g/P}(x_1^0, \mu_f) f_{g/P}(x_2^0, \mu_f) \left( 2N_c \ln \frac{m^2}{q_T^2} - 2\beta_0 \right) \right\}$$

$$\begin{aligned}
& + (P_{gg} \circ f)_{g/P}(x_1^0, \mu_f) f_{g/P}(x_2^0, \mu_f) + f_{g/P}(x_1^0, \mu_f) (P_{gg} \circ f)_{g/P}(x_2^0, \mu_f) \\
& + (x_1^0 \leftrightarrow x_2^0) \Big\}, \tag{70}
\end{aligned}$$

$$\begin{aligned}
\frac{d\sigma_{q\bar{q}}}{dq_T^2 dy}(\text{asym}) &= \sigma_{q\bar{q}}^0 \frac{\alpha_s}{2\pi} \frac{\tau_0}{q_T^2} \left\{ f_{q/P}(x_1^0, \mu_f) f_{\bar{q}/P}(x_2^0, \mu_f) \left( 2C_F \ln \frac{m^2}{q_T^2} - 3C_F \right) \right. \\
& + (P_{qq} \circ f)_{\bar{q}/P}(x_2^0, \mu_f) f_{q/P}(x_1^0, \mu_f) + f_{\bar{q}/P}(x_2^0, \mu_f) (P_{qq} \circ f)_{q/P}(x_1^0, \mu_f) \\
& \left. + (x_1^0 \leftrightarrow x_2^0) \right\}, \tag{71}
\end{aligned}$$

$$\begin{aligned}
\frac{d\sigma_{gg}}{dq_T^2 dy}(\text{asym}) &= \sigma_{q\bar{q}}^0 \frac{\alpha_s}{2\pi} \frac{\tau_0}{q_T^2} \left[ f_{q/P}(x_1^0, \mu_f) (P_{gg} \circ f)_{q/P}(x_2^0, \mu_f) \right] \\
& + \frac{1}{2} \sigma_{gg}^0 \frac{\alpha_s}{2\pi} \frac{\tau_0}{q_T^2} \left[ f_{g/P}(x_1^0, \mu_f) (P_{gg} \circ f)_{g/P}(x_2^0, \mu_f) \right] + (x_1^0 \leftrightarrow x_2^0), \tag{72}
\end{aligned}$$

where  $\sigma_{gg}^0 \equiv \frac{\pi}{16\Lambda_\pi^2}$  and  $\sigma_{q\bar{q}}^0 \equiv \frac{\pi}{24\Lambda_\pi^2}$ . The result of  $\frac{d\sigma_{q\bar{q}}}{dq_T^2 dy}(\text{asym})$  is similar to the one of  $\frac{d\sigma_{gg}}{dq_T^2 dy}(\text{asym})$ , and thus omitted here.

#### IV. NUMERICAL RESULTS

As mentioned in Section I, there are two additional free inputs in the RS model:  $m_1$  and  $k/\overline{M}_P$ , which have the following constraints:  $0.01 \leq k/\overline{M}_P < 0.1$  and  $\Lambda_\pi = \frac{m_1 \overline{M}_P}{x_1 k} \leq 10 \text{ TeV}$ . In our numerical calculations, for convenience, we choose the input parameters as  $\Lambda_\pi$  and  $m_1$ . For  $\Lambda_\pi = 4(8) \text{ TeV}$ , from current constraints, we have  $150 \text{ GeV} < m_1 < 1.5 \text{ TeV}$  ( $300 \text{ GeV} < m_1 < 3 \text{ TeV}$ ).

Moreover, for the NLO total cross sections  $\sigma^{(NLO)}$  and the contributions from different parts (including  $\sigma_{gg}^{(NLO)}$ ,  $\sigma_{q\bar{q}}^{(NLO)}$  and  $\sigma_{gq}^{(NLO)} + \sigma_{g\bar{q}}^{(NLO)}$ ), the NLO ( $\overline{\text{MS}}$ ) PDFs [24] is used throughout this paper. For the LO results, we define two cross sections as following:

$$\sigma^{(\text{LO1})} : \quad \text{LO partonic cross section convoluted with NLO } (\overline{\text{MS}}) \text{ PDFs}; \tag{73}$$

$$\sigma^{(\text{LO2})} : \quad \text{LO partonic cross section convoluted with LO PDFs}, \tag{74}$$

and correspondingly two  $K$  factors:

$$K_1 = \frac{\sigma^{(\text{NLO})}}{\sigma^{(\text{LO1})}}, \quad K_2 = \frac{\sigma^{(\text{NLO})}}{\sigma^{(\text{LO2})}}. \tag{75}$$

As the above definitions,  $K_1$  measures only the size of the NLO QCD corrections to the cross sections, while  $K_2$  accounts for the effects of changing parton distribution functions

additionally. As for the renormalization and factorization scales, we always choose  $\mu_r = \mu_f = m_n$ , unless otherwise specified.

In Fig. 7, we show the dependence of the total cross sections of  $pp \rightarrow h_{\mu\nu}^{(1)}$  at the LHC as functions of  $m_1$ , assuming  $\Lambda_\pi = 4 \text{ TeV}$ . The NLO and LO total cross sections decrease when  $m_1$  increases. The LO total cross sections are in general over several pb, and reach 100 pb when  $m_1 = 500 \text{ GeV}$ . Moreover, the figure also shows that the NLO QCD corrections enhance significantly the LO total cross sections, which are in general several tens percent.

Fig. 8 shows the dependence of the K factors on  $m_1$ , based on the results in Fig. 7. When  $m_1$  varies from 500 GeV to 1.5 TeV, the  $K_1$  factor ranges from 1.46 to 1.44, and the  $K_2$  factor ranges from 1.61 to 1.71. In addition, we give the different parts of the  $K_1$  factor, which show that the contributions from  $\sigma_{gg}^{(NLO)}$  ranges from 0.51 to 0.44, the contributions from  $\sigma_{q\bar{q}}^{(NLO)}$  range from 0.03 to 0.14, and the contributions from  $\sigma_{gq}^{(NLO)} + \sigma_{g\bar{q}}^{(NLO)}$  range from -0.08 to -0.14, respectively.

Fig. 9 shows the dependence of the total cross sections of  $pp \rightarrow h_{\mu\nu}^{(1)}$  at the LHC on the renormalization scale ( $\mu_r$ ) and the factorization scale ( $\mu_f$ ), assuming  $\mu_r = \mu_f$ ,  $\Lambda_\pi = 4 \text{ TeV}$  and  $m_1 = 1 \text{ TeV}$ . The scale dependence of the NLO total cross section is much smaller than that of the LO cross section. For example, the LO cross sections  $\sigma^{(LO1)}$  ( $\sigma^{(LO2)}$ ) vary by  $\sim \pm 17.8\%$  ( $\sim \pm 17.3\%$ ), when  $\mu_r = \mu_f$  ranges between 500 GeV and 4 TeV, while the NLO ones vary by  $\sim \pm 9.3\%$ . Moreover, we also give the scale dependence of the different parts in  $\sigma^{(NLO)}$ , for example, when  $\mu_r (= \mu_f)$  ranges between 500 GeV and 4 TeV,  $\sigma_{gg}^{(NLO)}$  varies from 4.5pb to 10.4pb,  $\sigma_{q\bar{q}}^{(NLO)}$  varies from 0.38pb to 0.93pb, and  $\sigma_{gq}^{(NLO)} + \sigma_{g\bar{q}}^{(NLO)}$  varies from 1.4pb to -3.5pb, respectively.

To estimate the uncertainties in the total cross sections due to the uncertainty of PDFs, we take the 41 sets of CTEQ6.1 PDFs to calculate the LO and NLO rates [25]. Fig. 10 shows the PDF uncertainties (defined here as the Eq. (3) in Ref. [26]) in the LO and NLO total cross sections for  $pp \rightarrow h_{\mu\nu}^{(1)}$  production at the LHC, as functions of  $m_1$ , assuming  $\Lambda_\pi = 8 \text{ TeV}$ . It turns out that the PDF uncertainties in the LO and NLO total cross sections increases as  $m_1$  increases. Moreover, when  $m_1$  is small ( $< 1.5 \text{ TeV}$ ), the PDF uncertainties in the LO and NLO total cross sections are about the same, while when  $m_1$  becomes large ( $> 1.5 \text{ TeV}$ ), the NLO rate has a larger uncertainty than the LO rate due to the PDF uncertainties, especially at large  $m_1$ .

Figs. 11 and 12 gives the transverse momentum distribution of  $h_{\mu\nu}^{(1)}$  from  $pp \rightarrow h_{\mu\nu}^{(1)}$  process

at the LHC, assuming  $\Lambda_\pi = 4 \text{ TeV}$ , for  $m_1 = 1 \text{ TeV}$  and  $2 \text{ TeV}$ , respectively. The peaks of the distribution appear at about  $18 \text{ GeV}$  and  $13 \text{ GeV}$ . The differential cross sections decrease sharply with the increase of  $q_T$ , which indicates that most events will happen in the relatively low  $q_T$  region, where the resummation effects are essential. Moreover, we also plot the various parts of the differential cross sections in Eq.(52). The perturbative and the asymptotic cross sections agree very well at small transverse momentum. On the other hand, the resummed and the asymptotic part are not canceled completely at high  $q_T$  due to the higher order effects included in the resummed one, so that the total one and the perturbative one will differ at large  $q_T$ . This can be considered as the theoretical uncertainties. In principle, one can return to the perturbative result for  $q_T > q_T^{\text{cut}}$ , where  $q_T^{\text{cut}}$  is arbitrarily chosen in the intermediate  $q_T$  region. However, in order to make the transition smooth, one must introduce some kinds of matching procedure which could also lead to uncertainties. In our work, as shown by Eq. (69), we subtract from the Y term the expansion of the resummed part of the same perturbative order, and this matching procedure between small  $q_T$  and large  $q_T$  region prevents double-counting of perturbative results and also guarantees a uniform theoretical accuracy over the entire  $q_T$  region[27].

From Eqs. (53), (54) and (69), we know that the transverse momentum distribution can be divided into three parts, i.e. the contributions from  $gg$ ,  $q\bar{q}$  and  $gq + g\bar{q}$  channels:

$$\frac{d\sigma}{dq_T^2 dy}(\text{total}) = \frac{d\sigma_{gg}}{dq_T^2 dy}(\text{total}) + \frac{d\sigma_{q\bar{q}}}{dq_T^2 dy}(\text{total}) + \frac{d\sigma_{gq+g\bar{q}}}{dq_T^2 dy}(\text{total}) \quad (76)$$

where

$$\frac{d\sigma_{gg}}{dq_T^2 dy}(\text{total}) \equiv \frac{d\sigma_{gg}}{dq_T^2 dy}(\text{resum}) + \frac{d\sigma_{gg}}{dq_T^2 dy}(\text{pert}) - \frac{d\sigma_{gg}}{dq_T^2 dy}(\text{asym}) \quad (77)$$

$$\frac{d\sigma_{q\bar{q}}}{dq_T^2 dy}(\text{total}) \equiv \frac{d\sigma_{q\bar{q}}}{dq_T^2 dy}(\text{resum}) + \frac{d\sigma_{q\bar{q}}}{dq_T^2 dy}(\text{pert}) - \frac{d\sigma_{q\bar{q}}}{dq_T^2 dy}(\text{asym}) \quad (78)$$

$$\begin{aligned} \frac{d\sigma_{gq+g\bar{q}}}{dq_T^2 dy}(\text{total}) &\equiv \frac{d\sigma_{g\bar{q}}}{dq_T^2 dy}(\text{pert}) + \frac{d\sigma_{gq}}{dq_T^2 dy}(\text{pert}) \\ &\quad - \frac{d\sigma_{g\bar{q}}}{dq_T^2 dy}(\text{asym}) - \frac{d\sigma_{gq}}{dq_T^2 dy}(\text{asym}) \end{aligned} \quad (79)$$

In Figs.13, 14 and 15, we thus plot these three contributions to the the transverse momentum distribution of  $h_\mu^{(1)}$  based on the results in Figs.11, respectively. We can see that for all these three parts, the perturbative and the asymptotic cross sections agree very well at small transverse momentum.

## V. CONCLUSIONS

In summary, we have calculated the next-to-leading order total cross section and transverse momentum distribution of single massive graviton production at the LHC in the RS model, including all-order soft gluon resummation effects. Our results show that the LO total cross sections are in general over several pb in most of the parameter space, and can reach 100 pb when  $m_1 = 500$  GeV. The NLO corrections enhance significantly the total cross sections, which is in general several tens percent, and reduce efficiently the dependence of the total cross sections on the renormalization/factorization scale. We have also examined the uncertainty in total cross sections due to the PDF uncertainties, and found that the uncertainty in NLO cross sections is slightly larger than that in LO ones, especially at large  $m_1$ . For the transverse momentum distribution, within the CSS resummation formalism, we resum the logarithmically-enhanced terms at small  $q_T$  to all orders up to NLO logarithmic accuracy. Combined with the fixed order calculations, we give consistent predictions for both small  $q_T$  and large  $q_T$ . Our results can be useful to the simulation of the events in the future collider experiments.

### Acknowledgments

We thank Yang Gao for useful discussion. This work was supported in part by the National Natural Science Foundation of China, under grants No. 10421503 and No. 10575001, the Key Grant Project of Chinese Ministry of Education under grant No. 305001.

- 
- [1] N. Arkani-Hamed et al., Phys. Lett. **B429**, 263 (1998); N. Arkani-Hamed et al., Phys. Rev. **D59**, 086004 (1999); N. Arkani-Hamed et al., Phys. Lett. **B436**, 257 (1998).
  - [2] L. Randall, R.Sundrum, Phys. Rev. Lett. **83**, 3370 (1999); L. Randall, R.Sundrum, Phys. Rev. Lett. **83**, 4690 (1999).
  - [3] J. Lykken, Phys. ReV. **D54**, 3693 (1996).
  - [4] E. Witten, Nucl. Phys. **B471**, 135 (1996).
  - [5] P. Horava and E. Witten, Nucl. Phys. **B460**, 506 (1996); Nucl. Phys. **B475** (1996) 94.
  - [6] I. Antoniadis, Phys. Lett. **B246**, 377 (1990).

- [7] C. Csaki, TASI Lectures on Extra Dimensions and Branes, hep-ph/0404096.
- [8] E. G. Adelberger [Eot-Wash Group Collaboration] hep-ex/0202008.
- [9] J.L. Hewett, Phys. Rev. Lett. **82** 4765 (1999).
- [10] H. Davoudiasl, et al., Phys.Rev.Lett. **84**, 2080 (2000).
- [11] JoAnne Hewett, Maria Spiropulu, Ann.Rev.Nucl.Part.Sci. **52**, 397 (2002).
- [12] Prakash Mathews et al., JHEP **0510**, 031 (2005); Prakash Mathews et al., Nucl.Phys. **B713**, 333 (2005); Prakash Mathews, V. Ravindran, hep-ph/0507250; M. C. Kumar et al., hep-ph/0604135.
- [13] B. C. Allanach, et al., JHEP **0212**, 039 (2002).
- [14] T. Han et al., Phys. Rev. **D59**, 05006 (1999).
- [15] W. Beenakker et al., Phys. Rev. **D40**, 54 (1989).
- [16] G. 't Hooft, M. J. G. Veltman, Nucl. Phys. **B44**, 189 (1972).
- [17] G. Altarelli et al., Nucl. Phys. **B157**, 461 (1979); J. C. Collins et al., in: Perturbative Quantum Chromodynamics, ed. A. H. Mueller (World Scientific, 1989).
- [18] B. W. Harris, J. F. Owens, Phys. Rev. **D65**, 094032 (2002).
- [19] G. Altarelli, G. Parisi, Nucl. Phys. **B126**, 298 (1977).
- [20] J. C. Collins, D. E. Soper and G. Sterman, Nucl. Phys. **B250**, 199 (1985).
- [21] R.P. Kauffman, Phys. Rev. **D44**, 1415 (1991).
- [22] P.B. Arnold, R.P. Kauffman, Nucl. Phys. **B349**, 381 (1991); C. Balázs et al., Phys. Lett. **B355**, 548 (1995).
- [23] F. Landry et al., Phys. Rev. **D67**, 073016 (2003).
- [24] J. Pumplin et al., JHEP **0207**, 012 (2002).
- [25] D. Stump et al., JHEP **0310**, 046 (2003).
- [26] J. Pumplin et al., JHEP 0207, 012(2002).
- [27] G. Bozzi, B. Fuks and M. Klasen, hep-ph/0603074.

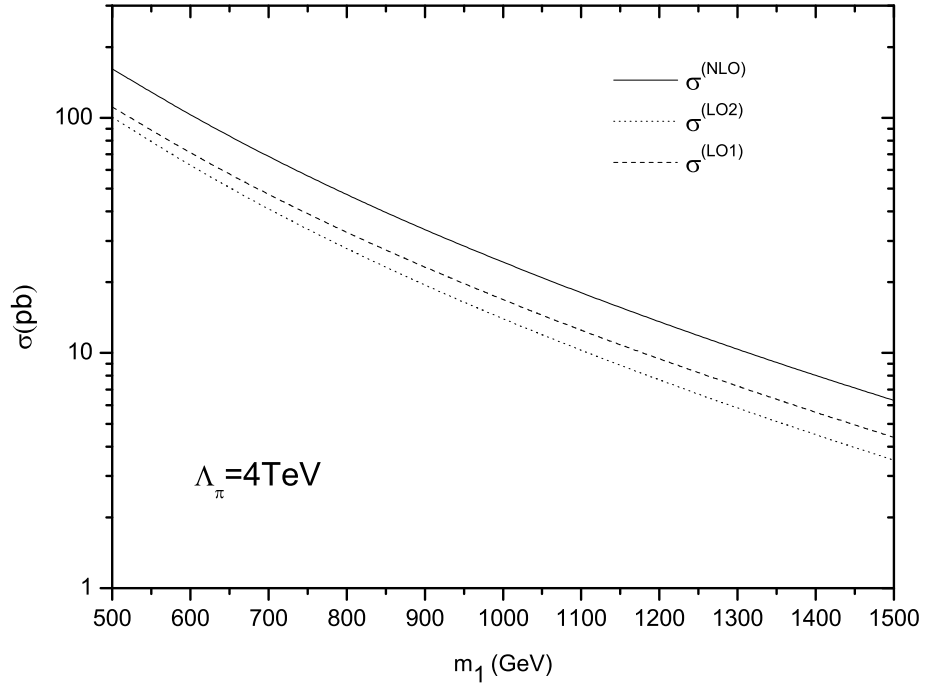


FIG. 7: Dependence of the total cross sections for the first KK graviton excitation mode direct production at the LHC on  $m_1$ .

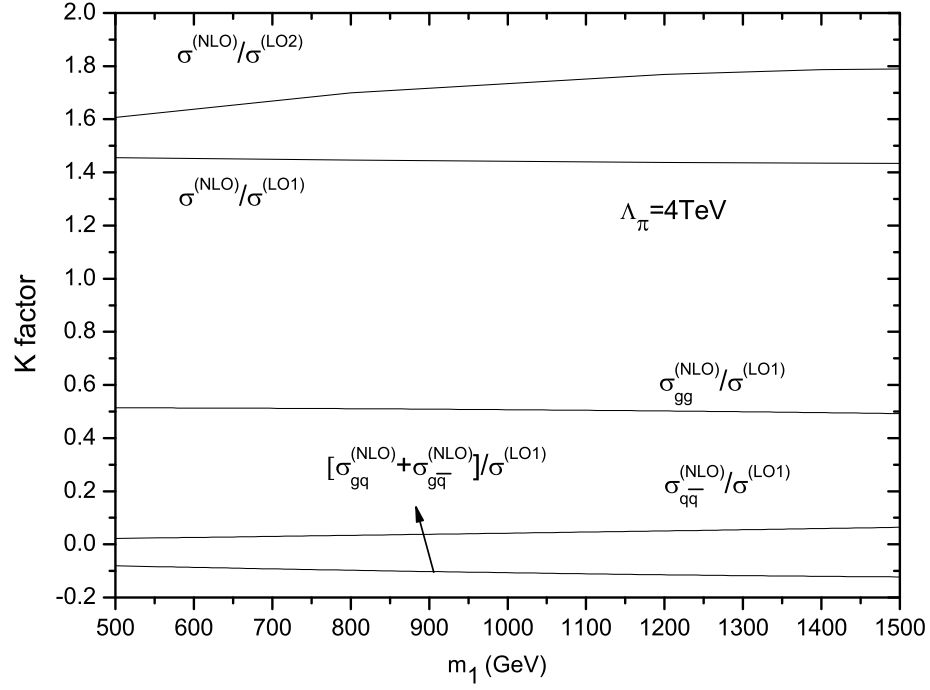


FIG. 8: Dependence of the  $K$ -factor on  $m_1$ , based on the results in Fig.7.

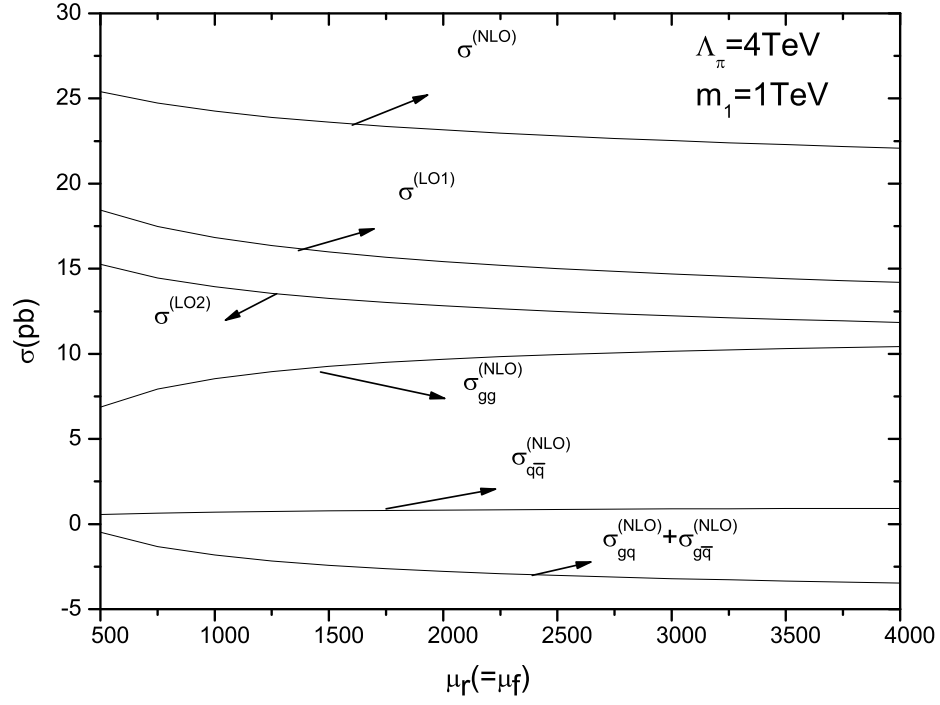


FIG. 9: Dependence of the total cross sections for the first KK graviton excitation mode direct production at the LHC on  $\mu_r = \mu_f$ .

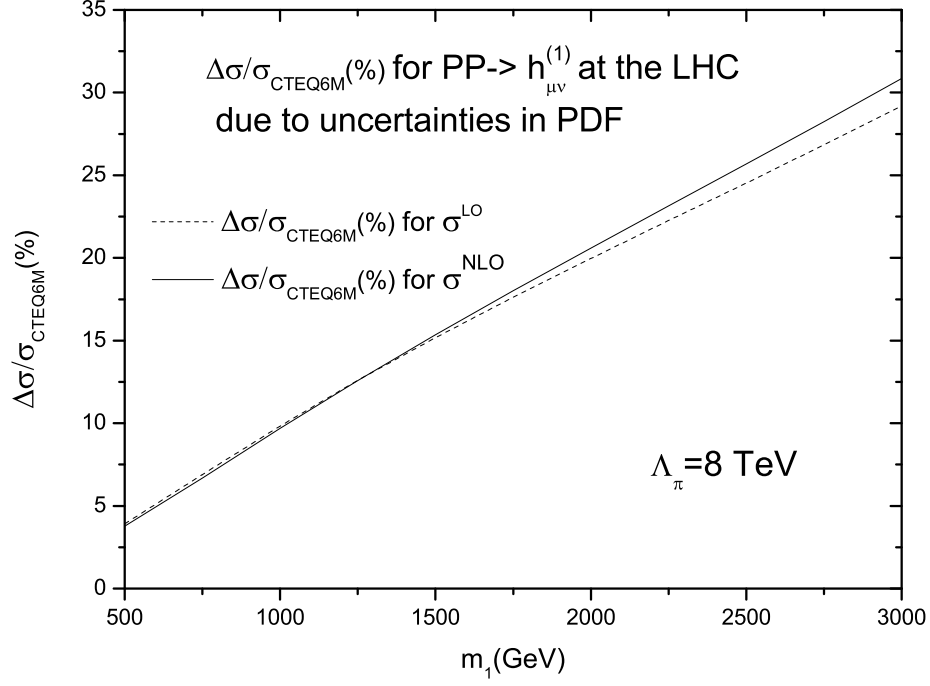


FIG. 10: The PDF dependence of the total cross sections for the first KK graviton excitation mode direct production at the LHC, as functions of  $m_1$ .

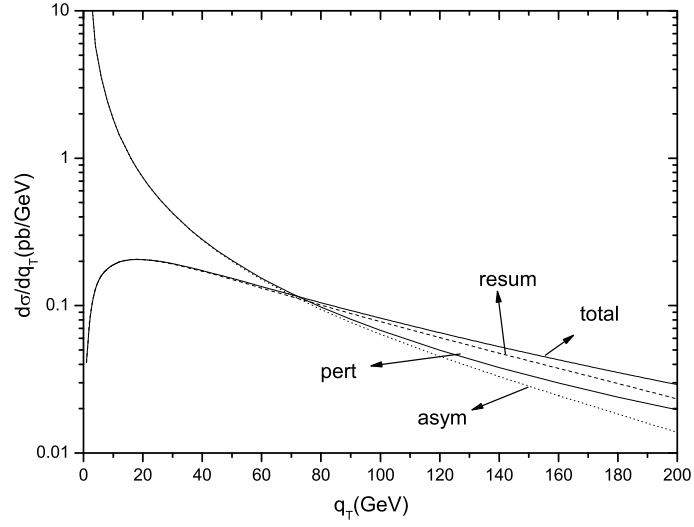


FIG. 11: The transverse momentum distribution of the first KK graviton excitation mode from  $pp \rightarrow h_{\mu\nu}^{(1)}$  process at the LHC, assuming  $\Lambda_\pi = 4 \text{ TeV}$  and  $m_1 = 1 \text{ TeV}$ .

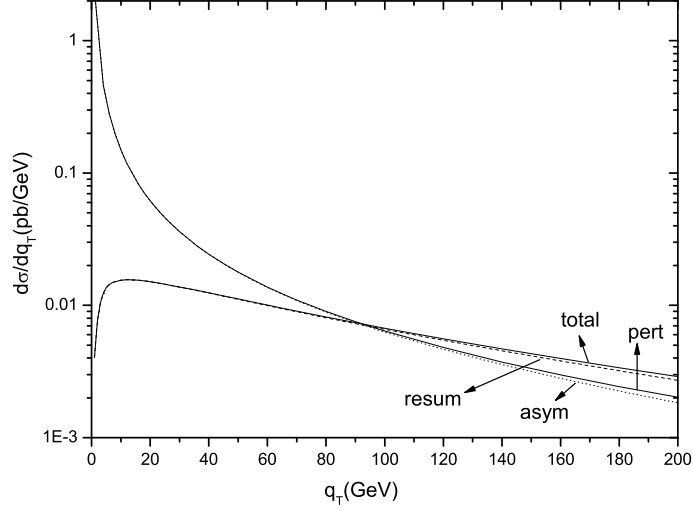


FIG. 12: The transverse momentum distribution of the first KK graviton excitation mode from  $pp \rightarrow h_{\mu\nu}^{(1)}$  process at the LHC, assuming  $\Lambda_\pi = 4$  TeV and  $m_1 = 2$  TeV.

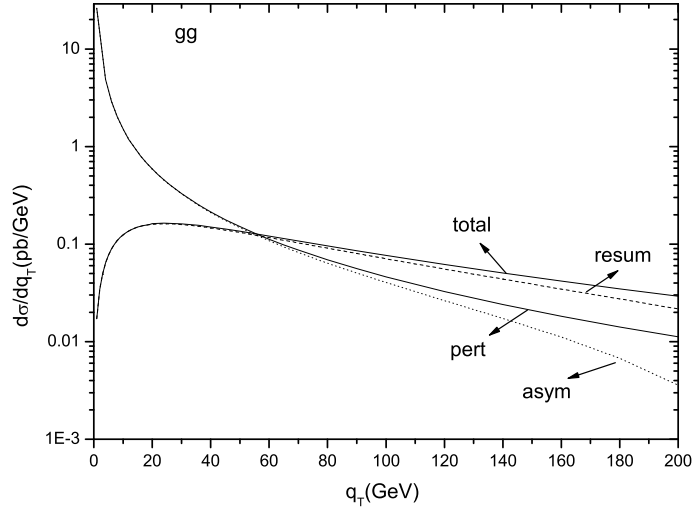


FIG. 13: The  $gg$  part of the transverse momentum distribution of the first KK graviton excitation mode, assuming  $\Lambda_\pi = 4$  TeV and  $m_1 = 1$  TeV.

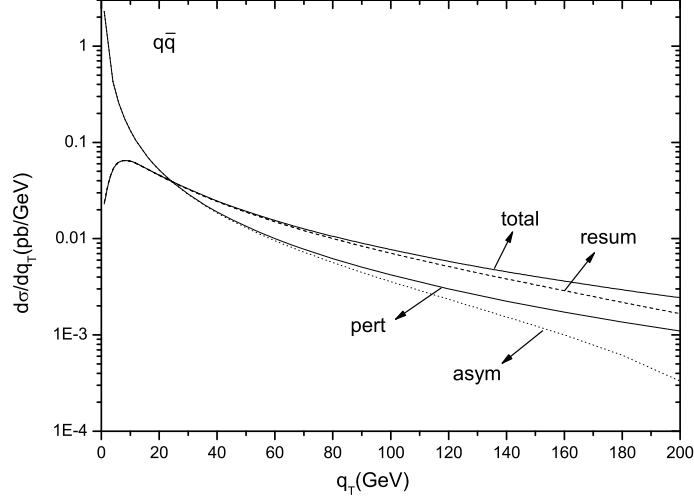


FIG. 14: The  $q\bar{q}$  part of the transverse momentum distribution of the first KK graviton excitation mode, assuming  $\Lambda_\pi = 4 \text{ TeV}$  and  $m_1 = 1 \text{ TeV}$ .

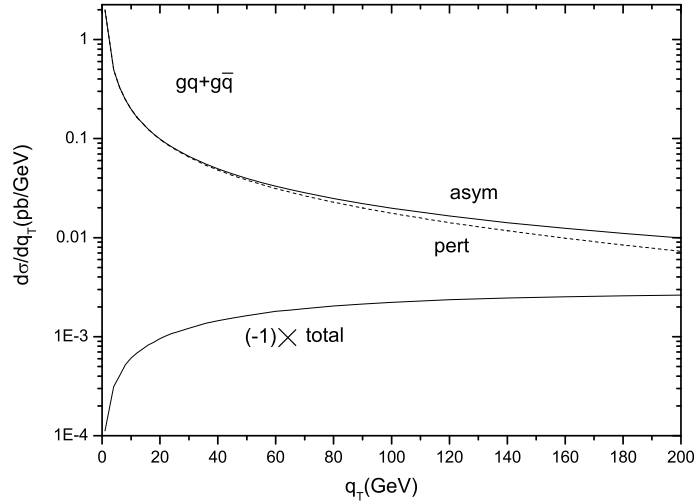


FIG. 15: The  $gq$  and  $g\bar{q}$  part of the transverse momentum distribution of the first KK graviton excitation mode, assuming  $\Lambda_\pi = 4 \text{ TeV}$  and  $m_1 = 1 \text{ TeV}$ .